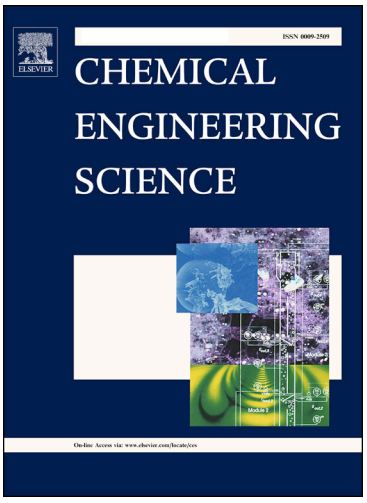

Highly efficient nickel-niobia composite catalysts for hydrogenation of CO_2 to methane

Edwin S. Gnanakumar, Narendraraj Chandran, Ivan V. Kozhevnikov, Aida Grau-Atienza, Enrique V. Ramos Fernández, Antonio Sepulveda-Escribano, N. Raveendran Shiju

PII: S0009-2509(18)30615-8
DOI: https://doi.org/10.1016/j.ces.2018.08.038
Reference: CES 14453

To appear in: *Chemical Engineering Science*

Received Date: 31 March 2018
Revised Date: 5 August 2018
Accepted Date: 18 August 2018

Please cite this article as: E.S. Gnanakumar, N. Chandran, I.V. Kozhevnikov, A. Grau-Atienza, E.V. Ramos Fernández, A. Sepulveda-Escribano, N. Raveendran Shiju, Highly efficient nickel-niobia composite catalysts for hydrogenation of CO_2 to methane, *Chemical Engineering Science* (2018), doi: https://doi.org/10.1016/j.ces.2018.08.038

Highly efficient nickel-niobia composite catalysts for hydrogenation of CO_2 to methane

Edwin S. Gnanakumar,[a] Narendraraj Chandran,[b] Ivan V. Kozhevnikov,[c] Aida Grau-Atienza,[d] Enrique V. Ramos Fernández,[d] Antonio Sepulveda-Escribano,[d] and N. Raveendran Shiju[a]*

[a] Van 't Hoff Institute for Molecular Sciences, University of Amsterdam, P.O. Box 94157, 1090GD Amsterdam, The Netherlands.

[b] Centre for Nano Science & Engineering, Indian Institute of Science, Bangalore, India

[c] Department of Chemistry, University of Liverpool, Liverpool L69 7ZD, UK.

[d] Departamento de Química Inorgánica-Instituto Universitario de Materiales de Alicante, Laboratorio de Materiales Avanzados, Universidad de Alicante, Apartado 99, 03080 Alicante, Spain

**Corresponding author:* n.r.shiju@uva.nl

Abstract

We studied the catalytic hydrogenation of CO_2 to methane using nickel-niobia composite catalysts. Catalysts containing 10-70 wt% Ni were synthesized by wet impregnation and tested for CO_2 hydrogenation in a flow reactor. 40 wt% was found to be the optimum Ni loading, which resulted in CO_2 conversion of 81% at 325^oC. We also calcined the Nb_2O_5 support at different temperatures to study the influence of calcination temperature on the catalytic performance. 40wt% Ni loaded on Nb_2O_5, which was pre-treated at 700^oC gave higher methanation activity (91% conversion of CO_2). Time on stream study for 50 h showed a stable activity and selectivity; thus confirming the scope for practical application.

Keywords: Niobia; CO_2 utilisation, methanation; nickel; heterogeneous catalysis; Methane.

1. Introduction

Increase in the concentration of CO_2 on earth atmosphere can cause various effects in the climate and is becoming a major threat to the living beings (Crowley 2000; Meehl et al., 2005). Therefore, significant efforts are being invested to deal with CO_2 emission and its consequences (Davis et al., 2010; P. Friedlingstein et al., 2010; Yang et al., 2008; Yu et al., 2008; Saeidi et al., 2014). Recently, in Paris, the United Nations conference on climatic change emphasized the importance of controlling the greenhouse gas emissions, particularly CO_2 (Rockström, et al., 2017). Simultaneous efforts are needed to decrease the CO_2 emission and for the active removal of CO_2 accumulated on earth atmosphere. Converting CO_2 into commercial chemicals and fuels is one of the practical ways for CO_2 mitigation (Saeidi et al., 2014, Daza et al., 2016, Porosoff et al., 2016). CO_2 hydrogenation to methane (synthetic natural gas/SNG) is one of the ways to do this (see equation below). Methane is a promising hydrogen carrier due to the well-established liquefaction of natural gas and its safe

transportation (Tada et al., 2012). Also this method integrates renewable resources (wind and solar energy) into the current energy mix efficiently. This is widely used in the power to gas concept (P2G) (Götz et al., 2016, Zhang et al., 2017), which was introduced for the conversion of renewable electrical power into a gaseous energy carrier such as methane. Since the surplus renewable power can be converted to gases, P2G will be important in the future energy system. The gases can be then used for transportation, domestic heating, feedstock and in power generation. P2G may not be feasible and economical in all locations, however, in Europe it is promising due to the increasing share of renewable electricity. P2G is a potential option to match the demand and supply of renewable power generation as the solar and wind-based power fluctuates. The existing gas infrastructure in Europe can accommodate large amounts of gas produced using this technology. Several European electrical companies have formed a consortium to implement this P2G concept. While P2G may not be favourable at all geographical locations, it is promising in European situation.

Further, methanation of CO_2 finds application in the process of ammonia production to purify the feed (Khorsand et al., 2007). Interestingly, methanation of CO_2 has been proposed to reduce the cost of manned exploration of Mars. In this proposal, H_2 can be transported to Mars from earth and will be reacted with atmospheric CO_2 to form methane and water. Methane can be stored as fuel and water will be electrolyzed to oxygen for life support. H_2 will be recycled for the methanation with CO_2 (Junaedi et al., 201, Wei et al., 2011). Moreover, its thermodynamic advantage makes methanation of CO_2 one of the promising processes for converting CO_2 into fuels (Aziz et al., 2015, Gao et al., 2012). This reaction is considerably faster than reactions to produce alcohols and other hydrocarbons (Aziz et al., 2015, Inui et al., 1991). Thus, this reaction gained more attention recently.

$$CO_2 + 4H_2 \rightleftharpoons CH_4 + 2H_2O \quad \Delta H = -165\ kJmol^{-1}$$

CO_2 hydrogenation was studied previously using a number of heterogeneous catalysts such as Rh, Ru, Pd, Ni, Co and mixed metals supported on metal oxides such as TiO_2, Al_2O_3, CeO_2 and ZrO_2 (Aziz et al., 2015, Frontera et al., 2017, Polanski et al., 2017, Wang et al., 2011). Among these metals, Ni based catalysts were investigated largely because of its abundance and low cost. They usually require more than 350^oC for high activity. However, at high temperatures, these catalysts deactivate rapidly due to Ni agglomeration, formation of volatile $Ni(CO)_4$ and coke deposition (Lu et al., 2014, Cai et al., 2013, Wachs et al., 2005, Zhou et al., 2015, Nie et al., 2017, Bajpai et al., 1982, Barrientos et al., 2014). Sometimes, selectivity towards methane is low due to the formation of by-products, particularly CO. Nature of the support plays an important role in metal supported catalyst, as the interaction between metal and support determines the activity and selectivity (Mejia et al., 2016, Batyrev et al, 2012). In general, high surface area supports are preferred for such reactions. Here, we use niobium pentoxide (niobia) as a support for nickel for CO_2 methanation reaction.

Niobium pentoxide is known for catalyzing several acid catalyzed reactions because of its acidity and stability in water as well as for redox and photocatalytic reactions (Nair et al., 2012, Nowak et al., 1999, Shiju et al., 2010). Niobia supported catalysts are widely studied for Fischer-Tropsch synthesis (den Otter et al., 2014, Frydman et al., 1999, den Otter et al., 2016), oxidation reactions (Jardim et al., 2015, Mozer et al., 2011, Rojas et al., 2009), and hydrodechlorination (Chary et al., 2004). A strong metal support interaction (SMSI) is observed for metals supported on niobia (Wojcieszak et al., 2006). This interaction could generate more active and selective sites, thus facilitating the reactions in the desired route. Hence, in our current work, we have chosen Nb_2O_5 as a support for CO_2 hydrogenation reaction. According to our knowledge, there is no previous report on CO_2 hydrogenation to methane using Nb_2O_5 as a support.

We impregnated niobia support with different amounts of Ni and screened them for methanation reaction. Among those, 40 wt% Ni loaded on Nb_2O_5 pre-treated at 700^oC showed maximum of 91% CO_2 conversion and >99% selectivity towards methane at 350^oC. The results suggest that the amount of nickel and calcination temperature of the support play important roles in the performance of catalysts. Time on stream (TOS) study shows that the same catalyst is stable and active up to 50h without any deactivation. Spent catalyst characterization shows the presence of nickel metallic particles, which were not changed in size significantly under reaction conditions.

2. Materials and Methods

2.1 Materials

All chemicals used in this work were used as received. Niobic acid was obtained from CBMM and $Ni(NO_3)_2.6H_2O$ was purchased from Alfa Aesar. Deionised water was used for all impregnation experiments.

2.2 Synthesis of catalysts

Nickel-niobia composite catalysts were synthesized by wet impregnation method. Before impregnation, niobic acid was calcined at 500 ^oC for 4 h to obtain Nb_2O_5. $Ni(NO_3)_2.6H_2O$ was used as the precursor for nickel. The synthesis procedure of 10 wt% Ni on Nb_2O_5 is given as an example: 1.98 g of $Ni(NO_3)_2.6H_2O$ was dissolved in 30 ml of water in a 200 ml round bottom flask. Then 3.6 g of Nb_2O_5 was added to the above solution. The whole mixture was kept stirring at 75 ^oC for 24 h. The obtained powder was further dried at 150 ^oC for 12 h. Finally, the powder was calcined at 400 ^oC to get 10 wt% Ni-Nb_2O_5 catalyst. Similarly, other loadings such as 20, 30, 40, 50 and 70 wt% Ni-Nb_2O_5 catalysts were synthesized. To study the effect of pre-treatment, we also calcined niobic acid at 700 ^oC and 900 ^oC before loading nickel. Final calcination of all catalysts was done at 400 ^oC. The catalysts are labelled as follows: nNi-Nb_2O_5-T (n is wt% of nickel and T is the pre-treatment temperature of Nb_2O_5). For comparison, we also used niobic acid as such as a support for 40 wt% Ni loading.

2.3 Instrumentation

X-ray diffraction patterns of the samples were recorded using Rigaku Miniflex II diffractometer using Ni-filtered Cu Kα (λ=1.5406 Å) radiation. The X-ray tube was operated at 30 kV and 15 mA. Measurements were recorded in the 2θ range from 10°- 80° with an angular step size of 0.05° and a counting time of 5°min^{-1}. Average crystallite size was calculated using Scherrer equation from the full width at half maximum (FWHM) of most intense XRD peak. Surface areas of the samples were determined by BET method using N_2 as adsorbent with multipoint modes at -196 °C. DRIFT (Diffuse Reflectance Infrared Fourier Transform) spectra of adsorbed pyridine were recorded on a Nicolet Nexus FTIR spectrometer using powdered 1:4 w/w catalyst mixtures with KBr. The catalyst-KBr mixtures were pre-treated at 150 °C/3×10^{-3} mmHg for 2 h, then exposed to pyridine vapour at room temperature for 1 h, followed by pumping out at 150 °C/3×10^{-3} mmHg for 1 h to remove physisorbed pyridine. The DRIFT spectra of adsorbed pyridine were recorded at room temperature at a 4 cm^{-1} resolution against 1:4 w/w catalyst-KBr mixture treated at 150 °C/3×10^{-3} mmHg for 2h. XPS spectra were collected using a Thermo Scientific K-ALPHA with Al-K radiation (1486.6 eV), monochromatized by a twin crystal monochromator, yielding a focused X-ray spot with a diameter of 400 µm, at 3 mA × 12 kV when charge compensation was achieved with the system flood gun that provides low energy electrons and low energy argon ions from a single source. The alpha hemispherical analyzer was operated in the constant energy mode with survey scan pass energies of 200 eV to measure the whole energy band and with 50 eV in a narrow scan to selectively measure the particular elements. An estimation of the intensities was done after a calculation of each peak integral, S-shaped background subtraction and fitting the experimental curve to a combination of a Lorentzian (30%) and Gaussian (70%) lines. Binding energies (BE), referenced to the C 1s line at 284.6 eV, have an accuracy of ± 0.1 eV. Temperature-programmed desorption of ammonia (NH_3-TPD) measurements were carried out in a U-shaped quartz reactor. An amount of 100 mg of each catalyst was first pre-heated at 200 °C with a He flow of 50 cm^3 min^{-1} for 1.5 h to remove the physisorbed

molecules. The sample was exposed to NH_3 gas flow of 50 cm^3 min^{-1} for 10 min at room temperature. Subsequently, the system was heated at 850 ºC with a heating rate of 10 ºC min^{-1}. The desorbed NH_3 was monitored by mass spectrometry. Transmission electron microscopy (TEM) images have been recorded using FEI-Thermo Fisher Scientific-Titan Themis 80-300kV FEG electron microscope operating at 300 kV. Samples were uniformly dispersed in isopropanol before depositing on carbon holy grid.

2.1 Catalytic activity test

Hydrogenation of CO_2 was carried out using a fixed bed catalytic reactor equipped with stainless steel tube reactor. The gas flows were controlled using mass flow controllers. 1 g of catalyst (20-40 mess size) was loaded inside the reactor. The catalysts were reduced in-situ using H_2:N_2 (2:3, v/v) gaseous mixture at 500 ^oC for 1 h before starting the reaction. Then the reactor temperature was adjusted to the desired reaction temperature. Subsequently, reaction mixture consisting of CO_2 and H_2 in the volumetric ratio of 1:4 was introduced into the reactor with the total flow rate of 12.5 ml/min. For experiments with different space velocity, the gas hourly space velocity (GHSV) was varied between 750/h and 20,600/h by changing the total flow rate of gas while keeping the catalyst mass constant. The outlet of the reactor was analyzed online using an Interscience Compact GC containing Porabond Q column and 5Å molecular sieve column and two TCD detectors.

3. Results and Discussion

CO_2 methanation reaction for all catalysts were carried out in the fixed bed reactor from 23°C to 450 ^oC (Figure 1a). Below 150 ^oC, no CO_2 conversion was observed. With increasing the temperature, CO_2 conversion increased and reached a maximum at 350°C. Among all catalysts, 40Ni-Nb_2O_5-500 catalysts showed highest conversion (81%) at 325 ^oC. When higher Ni loading was used, CO_2 conversion was still good, though lower than that of 40-Ni-Nb_2O_5-500 catalyst. All catalysts showed more than 99% selectivity towards CH_4 at maximum CO_2 conversion. After >350 ^oC, CO formation is favored and the CO_2 conversion is decreased due to reverse water-gas shift

reaction. Pure Nb_2O_5 did not give any CO_2 conversion at 350 ^oC; thus nickel is necessary to catalyse the reaction. Since 40Ni-Nb_2O_5-500 catalyst was most active, we chose this catalyst for further studies.

Powder XRD patterns of Ni-Nb_2O_5 catalysts are shown in Fig. 2a. Nb_2O_5 can exist in different polymorphic forms upon the heat treatment (Nair et al., 2012). After the calcination at 500 ^oC, Nb_2O_5 shows strong diffraction peaks at 2θ values of 22.6^o, 28.7^o, 36.9^o, 46.3^o, 50.8^o and 55.4^o which can be indexed as (001), (100), (101), (002), (110) and (102) respectively (JCPDS no. 28-0317) of Nb_2O_5 pseudo hexagonal phase. After loading nickel on Nb_2O_5, new peaks were observed (inset Fig 1) at 2θ values of 37.2^o, 43.4^o and 62.9^o, which can be assigned to (111), (200) and (220) respectively (JCPDS no. 47-1049) of face centered cubic NiO.

We also characterized the catalysts after the CO_2 hydrogenation reaction by powder XRD (Fig 2b). The diffraction pattern for the spent catalyst shows that the pseudo hexagonal structure of Nb_2O_5 remains unaltered. However, peaks corresponding to NiO were vanished and new diffraction patterns were observed at 2θ values of 44.5^o (111), 51.9^o (200) and 76.3^o (220). This indicates that NiO is converted to metallic Ni with face centered cubic structure (JCPDS no. 04-0850) after the reaction.

Nb_2O_5 is known for its variable acidic properties and phase transformation when it is heated. To check the influence of thermal treatment of the support on CO_2 methanation, we calcined the niobic acid at different temperatures (500 ^oC, 700 ^oC and 900 ^oC) and then impregnated nickel (40%) on these supports. The CO_2 methanation results are shown in Fig 1b. For a better comparison, we plotted T_{50} (temperature at which 50% CO_2 conversion was obtained) in this figure. The catalyst prepared using the support calcined at 700 °C i.e., 40Ni-Nb_2O_5-700 showed maximum CO_2 conversion (92% at around 350 ^oC). Highest T_{50} was obtained for 40Ni-Niobic acid (282 ^oC). The T_{50} follows the order, 40Ni-Nb_2O_5-700 < 40Ni-Nb_2O_5-900 < 40Ni-Nb_2O_5-500 < 40Ni-Niobic acid.

When Nb_2O_5 is subjected to high temperature treatment, three changes can be expected, i.e., change in crystal structure, change in acidity and change in the surface area. Figure 3 shows the XRD patterns of 40Ni-Nb_2O_5 catalyst calcined at different temperatures. Without calcination, no strong diffraction peaks of the support are obtained, showing the amorphous nature of the support. Hence, 40Ni-Niobic acid catalyst shows only the diffractions corresponding to fcc NiO. 40Ni-Nb_2O_5-500 catalyst shows diffraction pattern of the pseudo hexagonal phase as explained above. For 40Ni-Nb_2O_5-700 catalyst, diffraction peaks at 2θ values of 22.6^o (001), 28.4^o(180), 28.9^o(200), 36.7^o(181), 46.2^o(002) and 55.2^o(182) (JPCPD no. 30-0873) are obtained. This shows that Nb_2O_5 has an orthorhombic structure. 40Ni-Nb2O5-900 catalyst shows additional peaks at 2θ values of 23.9^o(100), 25.7^o(402) and 47.1^o(704), corresponding to monoclinic phase of Nb_2O_5 (JCPDS no. 37-1468). Thus, 40Ni-Nb_2O_5-900 contains a mixture of orthorhombic and monoclinic phases. Irrespective of the different polymorphs of Nb_2O_5, all catalysts show diffraction peaks of face centered cubic NiO.

To check the efficiency of the 40Ni-Nb_2O_5-700 catalyst at higher flow rates of the feed, we carried out CO_2 methanation at a WHSV of 20,600/h. As shown in Fig. 4, the CO_2 conversion kinetics was similar. Maximum CO_2 conversion (89%) was obtained at 350 °C which is almost same as the CO_2 conversion at a WHSV of 750/h. Selectivity towards CH_4 was more than 99% at 350^{o}C. We also did time on stream studies for 50h using 40Ni-Nb_2O_5-700 catalyst (Fig. 5). The CO_2 conversion and selectivity for CH_4 were unaltered. This shows that the catalyst is highly resistant to coke formation. Thermogravimetry measurement (not shown), showed only small amount of coke on the catalyst after 50 h of reaction. Please note that we only report a simple analysis here; however, thermogravimetric study can be more complicated. The oxidation of Ni to NiO can lead to a weight gain, which could interfere with the weight loss due to coke removal. The diffusion of coke into the subsurface/bulk was observed for Pd in previous studies and it cannot be ruled out for Ni without further detailed studies; however, this is out of the scope of this paper.

We characterized the catalysts with various techniques to correlate the catalytic activity with the catalyst structure. Table 1 shows the BET surface areas of the catalysts. 40Ni-Niobic acid and 40Ni-Nb_2O_5-500 catalysts have same surface area of 57 m^2/g. As the pre-treatment temperature of niobia increased, the surface area started to decrease. 40Ni-Nb_2O_5-700 and 40Ni-Nb_2O_5-900 catalysts had similar surface areas, which are much lower than the catalysts calcined at lower temperature, as expected. Despite having low surface area, 40Ni-Nb_2O_5-700 catalyst showed the best activity, indicating that the surface area has no direct correlation with activity in this case. The crystallite sizes of the calcined catalysts were calculated by the Scherrer equation using the most intense diffraction peaks of nickel and niobia. Table 1 shows these values. Niobic acid was amorphous; so no value is reported for this. For samples calcined at higher temperatures, the crystallite size increases with increasing calcination temperature, indicating higher crystallinity. Since the calcination was done at the same temperature after loading nickel, the crystallite size of nickel does not vary significantly. Please note that the absolute values may not be accurate, since several factors can influence the peak width in XRD. Instead, we can use these numbers as an indication of the trend of crystallite sizes. The values show that there is no significant difference in crystallite sizes of Ni when it is loaded on niobia calcined at temperatures of 500 °C or 700 °C or uncalcined. Thus, the crystallite size is not a major factor in determining the catalytic activity. However, when Ni is loaded on niobia calcined at 900 °C, a smaller crystallite size is observed. The Ni/Nb atomic ratio obtained from XPS increased with the calcination temperature of niobia indicating that there is a surface enrichment of nickel. Though 40Ni-Nb_2O_5-900 shows the highest surface enrichment of Ni, it is not the most active catalyst which prevents a direct correlation of surface Ni content with the activity. A direct correlation with a single catalyst characteristic seems to be not possible; thus, the activity may be determined by a combination of characteristics.

The acidity of the catalyst can be significantly affected by the temperature of the heat treatment. Hence, strength of the acid sites in 40wt%Ni loaded niobia catalysts were analyzed by temperature programmed

desorption of ammonia between 30 ^{o}C and 900 ^{o}C (Fig. 6). The NH_3-TPD profiles of 40Ni-Nb_2O_5-T catalysts showed a low temperature desorption peak, which can be assigned to the interaction of NH_3 molecules with weak acid sites. The peak at 500 ^{o}C observed for 40Ni-Niobic acid catalyst could be due to the dehydroxylation of the surface –OH groups of niobic acid (Marakatti et al., 2016). NH_3 desorption peak observed around 700 ^{o}C can be assigned to the presence of strong acidic sites in the catalysts. Total acidic sites are decreased as the niobia pre-treatment temperature increases. This is due to the decrease in the surface area of the catalysts and dehydroxylation of surface hydroxyl groups at high temperature. 40Ni-Nb_2O_5-700 and 40Ni-Nb_2O_5-900 catalysts contain higher concentration of strong acidic sites than weak acidic sites. In 40Ni-Nb_2O_5-700 catalyst, desorption of NH_3 from strong acid sites occurred at higher temperature (maximum desorption around 700 ^{o}C) compared with 40Ni-Nb_2O_5-900 catalyst (630 ^{o}C). To study the contribution from Brønsted and Lewis acidities, we did the DRIFT-IR study of pyridine adsorbed on 40Ni-Nb_2O_5-T catalysts (Fig.7). The DRIFT spectra obtained are of rather low quality for a quantitative analysis, probably because of the high Ni loading (40%). However, qualitatively, we can infer that the Lewis acidity (L) dominates in these samples. The density of acid sites, both Lewis (L) and Brønsted (B), decreases with the temperature of pretreatment, with the B/L ratio practically unchanged (B/L = 0.28-0.32). Both techniques confirm that high temperature treated catalyst contains more Lewis acid sites. The catalysts with strong acid sites are also better in terms of catalytic performance; however, it is difficult to assign a reason for this.

Ni $2p_{3/2}$ XPS of 40Ni-Nb_2O_5-T samples are shown in Fig 8a. 40Ni-Niobic acid catalyst shows a multiplet split at 853.9, 855.7 and 858.4eV. These peaks are characteristic of Ni^{2+} species. Absence of a peak at 852.7 eV confirms there is no metallic Ni species in this sample. As the pre-treatment temperature of Nb_2O_5 changes, there is a change in the peak ratio of the multiplet. Since the multiplets are usually ascribed to the interference in the electron core levels, the change observed here shows that the electron density of nickel center varies. This could be due to an interaction

between the support and NiO. This also indicates that there is a stronger metal-support interaction when the support is pre-treated at higher temperatures.

Similar trends were not clearly seen in the XPS of Nb core level. It is because the Nb has less electrons in the d level and changes are more difficult to be observed. Fig 8b shows the comparison of Ni $2p_{3/2}$ peaks of fresh and spent 40Ni-Nb_2O_5-700 catalysts. Ni$2p_{3/2}$ multiplet of spent catalyst (852.1 eV) is observed at lower BE than the fresh catalyst (852.9). This shows that the Ni is in a reduced state during the reaction. Ni/Nb atomic ratios in different catalysts are shown in Table 1. As pre-treatment temperature increases, the amount of Ni on the surface is higher. 40Ni-Nb_2O_5-900 catalyst contains highest Ni/Nb surface ratio of 12.7. 40Ni-Nb_2O_5-700 catalyst, which is the most active, has Ni/Nb ratio of 3.93. Other two catalysts have lower Ni/Nb ratios. O1s spectra of 40Ni-Nb_2O_5-T catalysts are shown in Fig 9. They can be deconvoluted into three different peaks corresponding to surface hydroxyl groups, oxygen bonded to Nb and oxygen bonded to Ni. The changes in the O 1s B.E. can be caused by different covalence degrees of the metal-oxygen bond, resulting in changes in the negative charge and basicity of the oxygen. 40Ni-Nb_2O_5-900 catalyst has more oxygen bonded with Ni compared to other catalysts.

TEM images of fresh and spent (after 50h of reaction) 40Ni-Nb_2O_5-700 catalysts are shown in Fig 10. NiO particles are (Fig. 10 (a) and (b)) present as rectangular slabs on Nb_2O_5. Figures 10 (c) and (d) show the images of spent 40Ni-Nb_2O_5-700 catalyst. There is no major agglomeration of Ni particles in spent 40Ni-Nb_2O_5-700 catalyst, indicating that the catalyst is stable during the reaction, in agreement with the long-term reaction study (Fig. 5). Ni-agglomeration starts happening however, and it may increase with further time on stream.

4. Conclusions

In this work, we prepared highly active and selective CO_2 methanation catalysts based on nickel and niobia. At atmospheric pressure and 350 °C, 40Ni-Nb_2O_5-700 catalyst gave CO_2 conversion of

92% and CH_4 selectivity of 99%. This shows that the pre-treatment temperature of the niobia support is important in determining the final catalyst performance. The catalyst showed a stable activity during a continuous test of 50 h. The pre-treatment temperature affects the density and strength of the acid sites on the final catalyst. Strong acid sites seems to be more favourable for the CO_2 hydrogenation, though we couldn't assign a direct reason for this.

Acknowledgment

E.S.G. and N.R.S acknowledge the financial support from NWO CAPITA project (732.013.002). ASE acknowledges the financial support from the MINECO projects MAT-2013-45008-P and MAT2016-81732-ERC. EVRF gratefully acknowledge support from MINECO for his Ramón y Cajal grant (RyC-2012-11427) and University of Alicante for the project GRE-13-31. Generalitat Valenciana is also acknowledged for financial support (PROMETEOII/ 2014/004).

References

1. Crowley, T. J. 2000. Causes of Climate Change Over the Past 1000 Years. Science 289, 270-277.
2. Meehl, G. A. W. M. Washington, W. D. Collins, J. M. Arblaster, A. X. Hu, L. E. Buja, W. G. Strand and H. Y. Teng, 2005. How Much More Global Warming and Sea Level Rise? Science 307, 1769-1772.

3. Davis, S. J., K. Caldeira and H. D. Matthews, Future CO_2 emissions and climate change from existing energy infrastructure., Science, 2010, 329, 1330-1333.

4. P. Friedlingstein, R. Houghton, G. Marland, J. Hackler, T. A. Boden, T. Conway, J. Canadell, M. Raupach, P. Ciais and C. Le Quere, 2010, Update on CO_2 emissions, Nature Geoscience, 3, 811-812.

5. H. Yang, Z. Xu, M. Fan, R. Gupta, R. B. Slimane, A. E. Bland and I. Wright, 2008, Progress in carbon dioxide separation and capture: A review, Journal of environmental sciences, 20, 14-27.

6. K. M. K. Yu, I. Curcic, J. Gabriel and S. C. E. Tsang, 2008, Recent advances in CO_2 capture and utilization, ChemSusChem, 1, 893-899.

7. S. Saeidi, N. A. S. Amin and M. R. Rahimpour, 2014, Hydrogenation of CO_2 to value-added products—A review and potential future developments. Journal of CO_2 utilization, 5, 66-81.

8. J. Rockström, O. Gaffney, J. Rogelj, M. Meinshausen, N. Nakicenovic, H. J. Schellnhuber, 2017, A roadmap for rapid decarbonization, Science, 355, 1269-1271.

9. Y. A. Daza and J. N. Kuhn, 2016, CO_2 conversion by reverse water gas shift catalysis: comparison of catalysts, mechanisms and their consequences for CO_2 conversion to liquid fuels, RSC Advances, 6, 49675-49691.

10. M. D. Porosoff, B. Yan and J. G. Chen, 2016, Catalytic reduction of CO_2 by H_2 for synthesis of CO, methanol and hydrocarbons: challenges and opportunities, Energy & Environmental Science, 9, 62-73.

11. S. Tada, T. Shimizu, H. Kameyama, T. Haneda and R. Kikuchi, 2012, Ni/CeO2 catalysts with high CO2 methanation activity and high CH4 selectivity at low temperatures, International Journal of Hydrogen Energy, 37, 5527-5531.

12. M. Götz, J. Lefebvre, F. Mörsa, A. M. Koch, F. Graf, S. Bajohr, R. Reimert, T. Kolb, 2016, Renewable Power-to-Gas: A technological and economic review, Renewable Energy, 85, 1371-1390.

13. X. Zhang, C. Bauer, C. L. Mutel, K. Volkart, 2017, Life Cycle Assessment of Power-to-Gas: Approaches, system variations and their environmental implications, Applied Energy, 190, 326-338.

14. K. Khorsand, M. A. Marvast, N. Pooladian and M. Kakavand, 2007, Modeling and simulation of methanation catalytic reactor in ammonia unit, Petroleum & Coal, 49, 46-53.

15. C. Junaedi, K. Hawley, D. Walsh, S. Roychoudhury, M. Abney and J. Perry, 2011, Compact and Lightweight Sabatier Reactor for Carbon Dioxide Reduction, 41st International Conference on Environmental Systems. Portland, Oregon.

16. W. Wei and G. Jinlong, 2011, Methanation of carbon dioxide: an overview, Frontiers of Chemical Science and Engineering, 5, 2-10.

17. M. A. A. Aziz, A. A. Jalil, S. Triwahyono and A. Ahmad, 2015, CO_2 methanation over heterogeneous catalysts: recent progress and future prospects, Green Chemistry, 17, 2647-2663.

18. J. Gao, Y. Wang, Y. Ping, D. Hu, G. Xu, F. Gu and F. Su, 2012, A thermodynamic analysis of methanation reactions ofcarbon oxides for the production of synthetic natural gas, RSC Advances, 2, 2358-2368.

19. T. Inui and T. Takeguchi, 1991, Effective conversion of carbon dioxide and hydrogen to hydrocarbons, Catalysis Today, 10, 95-106.

20. P. Frontera, A. Macario, M. Ferraro and P. Antonucci, 2017, Supported Catalysts for CO2 Methanation: A Review, Catalysts, 7, 59.

21. J. Polanski, T. Siudyga, P. Bartczak, M. Kapkowski, W. Ambrozkiewicz, A. Nobis, R. Sitko, J. Klimontko, J. Szade and J. Lelątko, 2017, Oxide passivated Ni-supported Ru nanoparticles in silica: A new catalyst for low-temperature carbon dioxide methanation, Applied Catalysis B: Environmental, 206, 16-23.

22. W. Wang, S. Wang, X. Ma and J. Gong, 2011, Recent advances in catalytic hydrogenation of carbon dioxide, Chemical Society Reviews, 40, 3703-3727.

23. H. L. Lu, X. Z. Yang, G. J. Gao, K. B. Wang, Q. Q. Shi, J. Wang, C. H. Han, J. Liu, M. Tong, X. Y. Liang and C. F. Li, 2014, Mesoporous zirconia-modified clays supported nickel catalysts for CO and CO2 methanation, International Journal of Hydrogen Energy, 39, 18894-18907.

24. W. Cai, Q. Zhong and Y. X. Zhao, 2013, Fractional-hydrolysis-driven formation of non-uniform dopant concentration catalyst nanoparticles of Ni/CexZr1− xO2 and its catalysis in methanation of CO_2, Catalysis Communications, 39, 30-34.

25. I. E. Wachs, 2005, Recent conceptual advances in the catalysis science of mixed metal oxide catalytic materials, Catalysis Today, 100, 79-94.

26. L. Zhou, Q. Wang, L. Ma, J. Chen, J. Ma and Z. Zi, 2015, CeO2 Promoted Mesoporous Ni/γ-Al2O3 Catalyst and its Reaction Conditions For CO2 Methanation, Catalysis Letters, 145, 612-619.

27. W. Nie, X. Zou, C. Chen, X. Wang, W. Ding and X. Lu, 2017, Methanation of Carbon Dioxide over Ni–Ce–Zr Oxides Prepared by One-Pot Hydrolysis of Metal Nitrates with Ammonium Carbonate, Catalysts, 7, 104.

28. P. K. Bajpai, N. N. Bakhshi and J. F. Mathews, 1982, Deactivation studies of nickel catalysts used in the methanation of carbon monoxide, Canadian Journal of Chemical Engineering, 60, 4-10.

29. J. Barrientos, M. Lualdi, M. Boutonnet and S. Jaras, 2014, Deactivation of supported nickel catalysts during CO methanation, Applied Catalysis a-General, 486, 143-149.

30. C. H. Mejia, E. S. Raja, A. Olivos-Suarez, J. Gascon, H. F Greer, W. Zhou, G. Rothenberg and N. R. Shiju, 2016, Ru/TiO_2-catalysed hydrogenation of xylose: the role of crystal structure of the support. Catal. Sci. Technol. 6, 577-582.

31. E. D. Batyrev, N. R. Shiju and G. Rothenberg, 2012, Exploring the Activated State of Cu/ZnO(0001)-Zn, a Model Catalyst for Methanol Synthesis. J. Phys. Chem. C, 116, 19335-19341.

32. G. S. Nair, E. Adrijanto, A. Alsalme, I. V. Kozhevnikov, D. J. Cooke, D. R. Brown and N. R. Shiju, 2012, Glycerol utilization: solvent-free acetalisation over niobia catalyst. Catal. Sci. Technol., 2, 1173-1179.

33. I. Nowak and M. Ziolek, 1999, Niobium Compounds: Preparation, Characterization, and Application in Heterogeneous Catalysis, Chemical Reviews, 99, 3603-3624.

34. N. R. Shiju, D. R. Brown, K. Wilson, G. Rothenberg, 2010, Glycerol valorization: dehydration to acrolein over silica-supported niobia catalysts. Top. Catal., 53, 1217-1223.

34. J. den Otter and K. P. de Jong, 2014, Highly Selective and Active Niobia-Supported Cobalt Catalysts for Fischer–Tropsch Synthesis, Topics in Catalysis, 57, 445-450.

35. A. Frydman, D. G. Castner, C. T. Campbell and M. Schmal, 1999, Carbon Monoxide Hydrogenation on Co–Rh/Nb2O5 Catalysts, Journal of Catalysis, 188, 1-13.

36. J. H. den Otter, H. Yoshida, C. Ledesma, D. Chen and K. P. de Jong, 2016, On the Superior Activity and Selectivity of PtCo/Nb2O5 Fischer-Tropsch Catalysts, Journal of Catalysis, 340, 270-275.

37. E. D. Jardim, S. Rico-Frances, Z. Abdelouahab-Reddam, F. Coloma, J. Silvestre-Albero, A. Sepulveda-Escribano and E. V. Ramos-Fernandez, 2015, High performance of Cu/CeO2-Nb2O5 catalysts for preferential CO oxidation and total combustion of toluene, Applied Catalysis a-General, 502, 129-137.

38. T. S. Mozer and F. B. Passos, 2011, Selective CO oxidation on Cu promoted Pt/Al2O3 and Pt/Nb2O5 catalysts, International Journal of Hydrogen Energy, 36, 13369-13378.

39. E. Rojas, M. O. Guerrero-Perez and M. A. Banares, 2009, Direct ammoxidation of ethane: An approach to tackle the worldwide shortage of acetonitrile, Catalysis Communications, 10, 1555-1557.

40. K. V. R. Chary, K. S. Lakshmi, P. V. R. Rao, K. S. R. Rao and M. Papadaki, 2004, Characterization and catalytic properties of niobia supported nickel catalysts in the hydrodechlorination of 1,2,4-trichlorobenzene, Journal of Molecular Catalysis a-Chemical, 223, 353-361.

41. R. Wojcieszak, A. Jasik, S. Monteverdi, M. Ziolek and M. M. Bettahar, 2006, Nickel niobia interaction in non-classical Ni/Nb2O5 catalysts, Journal of Molecular Catalysis a-Chemical, 256, 225-233.

42. V. S. Marakatti, P. Manjunathan, A. B. Halgeri and G. V. Shanbhag, 2016, Catalysis Science & Technology, 6, 2268-2279.

Table 1. Physico-chemical properties of 40Ni-Nb_2O_5-T* catalysts

Catalyst	Pretreatment temperature of Nb_2O_5	BET surface area (m^2/g)	NiO crystallite size (nm)**	Nb_2O_5 crystallite size (nm) **	Ni/Nb atomic ratio	T_{50} CO_2 conversion (^oC)
40Ni-Niobic acid	--	57	30	--	1.50	282
40Ni-Nb_2O_5-500	500^{o}C	57	30	18	1.89	274
40Ni-Nb_2O_5-700	700^{o}C	11	32	32.5	3.93	242
40Ni-Nb_2O_5-900	900^{o}C	16	26	38	12.7	261

*T = calcination temperature
**calculated using Scherrer´s equation with the most intense peak.

Figure Captions

Fig. 1 (a) CO_2 methanation results for Ni/Nb_2O_5 catalysts with different Ni loading and (b) $40Ni\text{-}Nb_2O_5$-T catalysts in fixed bed reactor with GHSV of 750/h.

Fig. 2 (a) Powder X-ray diffraction patterns of 10-40 wt% $Ni\text{-}Nb_2O_5$-500 catalysts calcined at 400 ^oC and **(b)** after CO_2 methanation reaction.

Fig. 3 Powder X-ray diffraction patterns of $40Ni\text{-}Nb_2O_5$-T catalysts. T indicates the calcination temperature of the support. All catalysts were calcined at 400^oC after nickel impregnation.

Fig. 4 CO_2 methanation results for $40Ni\text{-}Nb_2O_5$-700 catalyst with a WHSV of 20,600/h.

Fig. 5 CO_2 methanation time on stream studies using $40Ni\text{-}Nb_2O_5$-700 catalyst. 1 g of catalyst was loaded in the fixed bed reactor and total of 50 ml/min gas flow (1:4 volumetric ratio of CO_2:H_2) was used in the methanation reaction.

Fig 6. The ammonia TPD of $40Ni\text{-}Nb_2O_5$-T catalysts. The pre-treatment temperature of the support has a strong influence on the concentration and strength of the acid sites.

Fig 7. DRIFT spectra of pyridine adsorbed on $40Ni\text{-}Nb_2O_5$-T catalysts. (1) 40Ni-Niobic acid (2) $40Ni\text{-}Nb_2O_5$-500 (3) $40Ni\text{-}Nb_2O_5$-700 and (4) $40Ni\text{-}Nb_2O_5$-900.

Fig 8. Ni $2p_{3/2}$ XPS of $40Ni\text{-}Nb_2O_5$-T catalysts. In (a) the pre-treatment temperature of the niobia support is different and in (b) the fresh and spent samples of $40Ni\text{-}Nb_2O_5$-700 are compared.

Fig 9. O 1s XPS of $40Ni\text{-}Nb_2O_5$-T catalysts. The spectra can be deconvoluted into three indicating the presence of three types of oxygen species.

Fig 10. TEM images of fresh [(a) and (b)] and spent [(c) and (d)] $40Ni\text{-}Nb_2O_5$-700 catalysts.

Figures

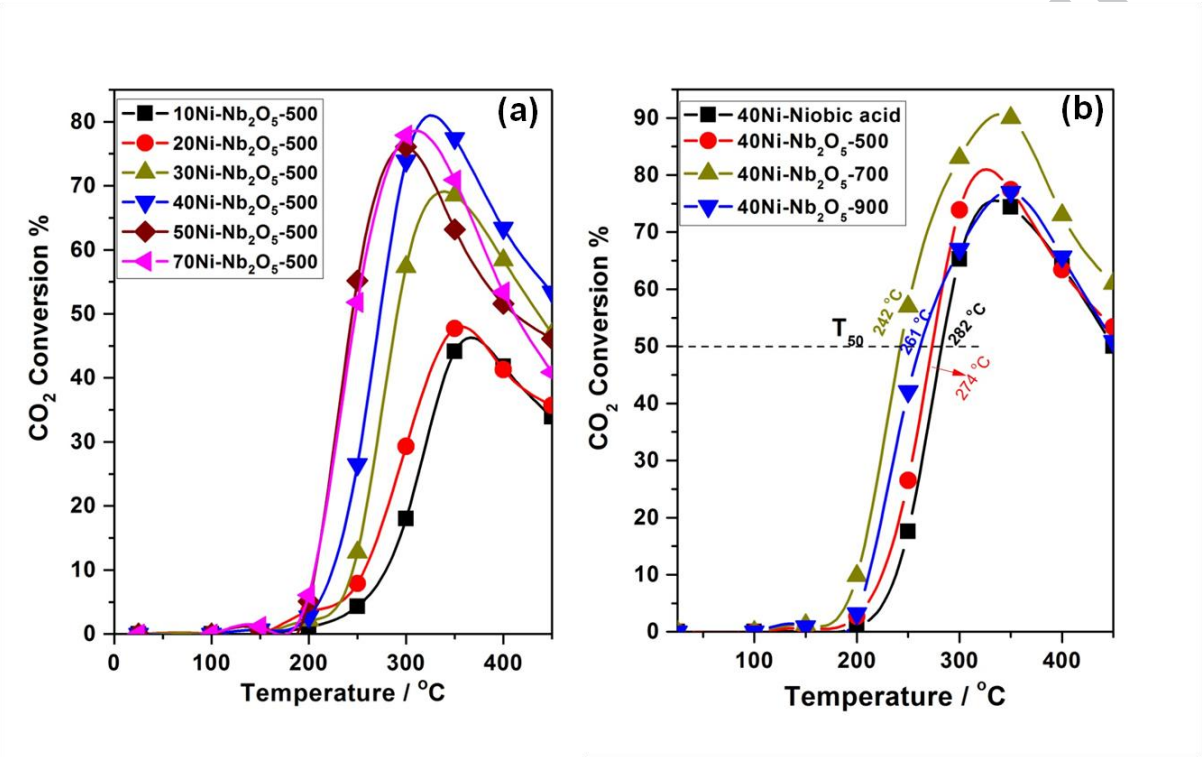

Figure 1.

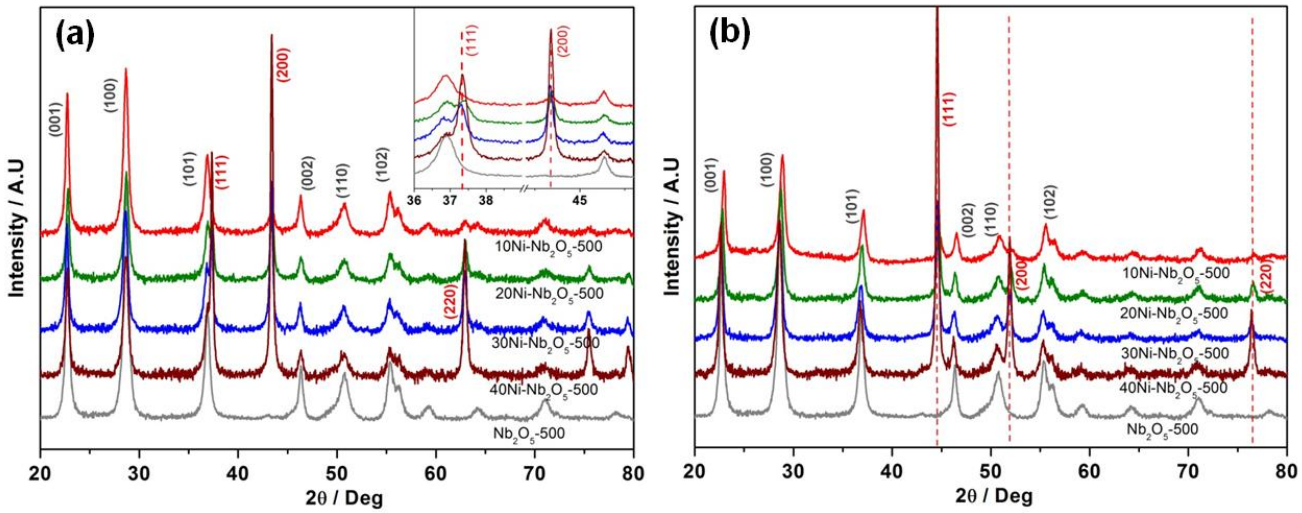

Figure 2

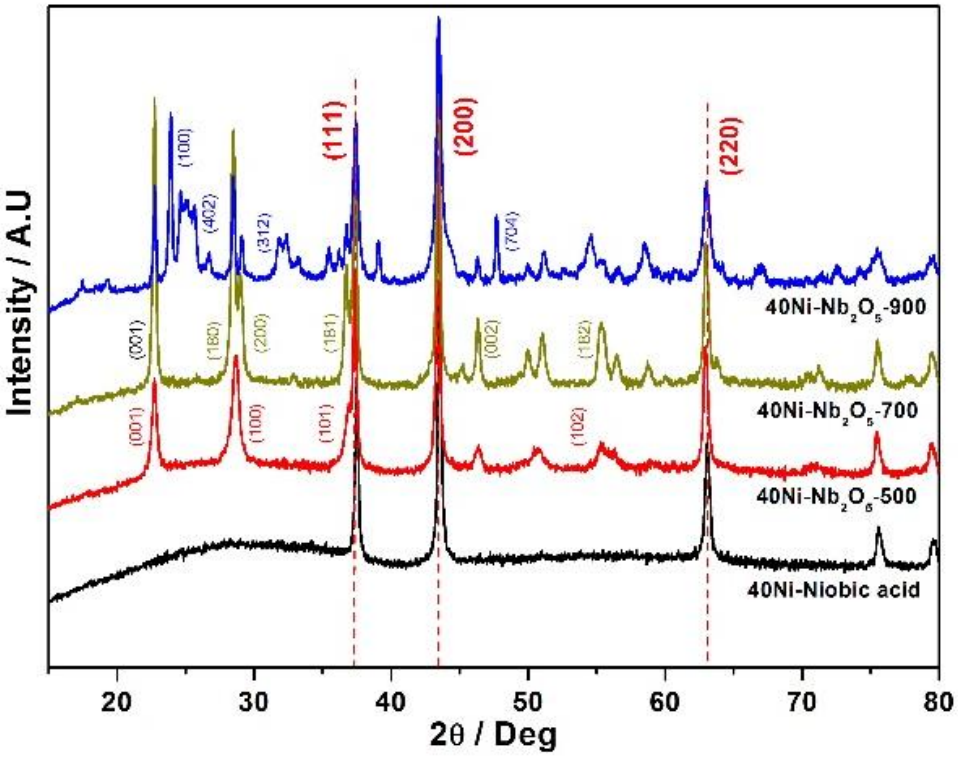

Figure 3

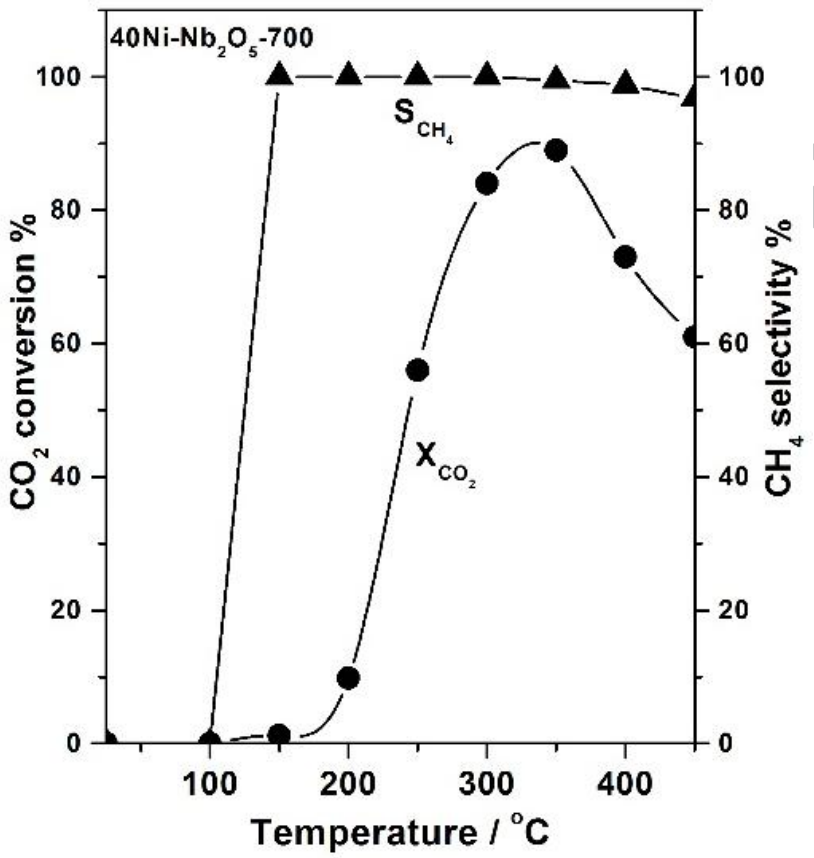

Figure 4

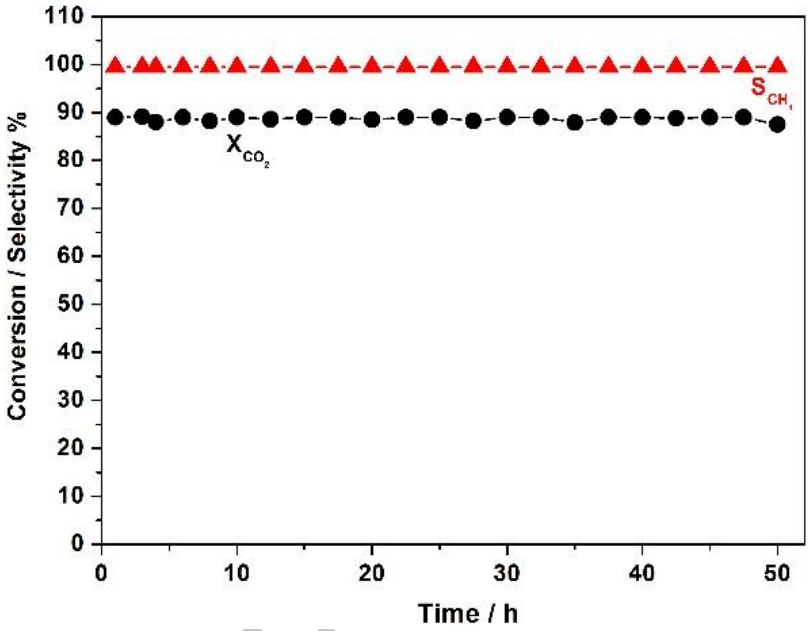

Figure 5

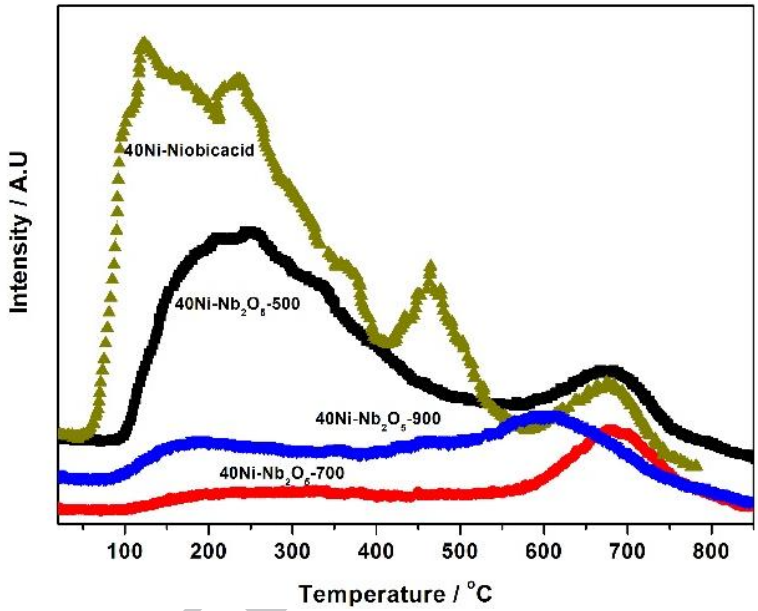

Figure 6

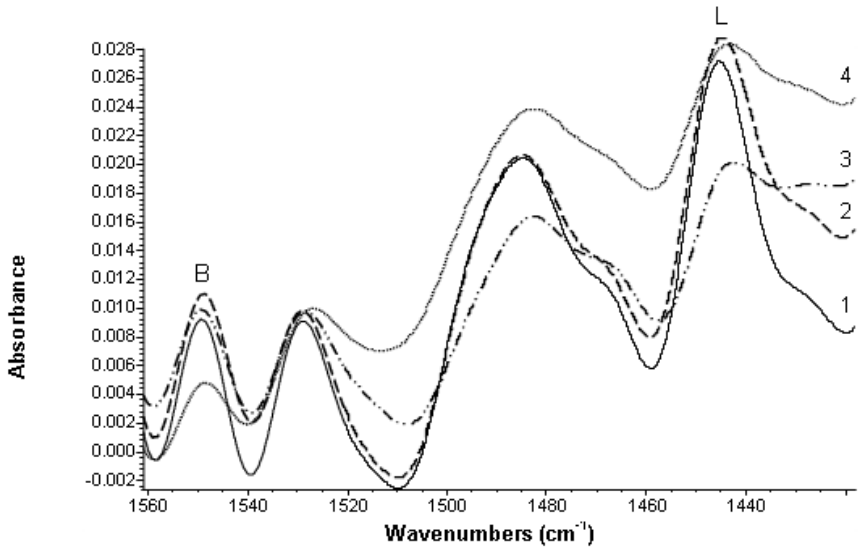

Figure 7

(a)

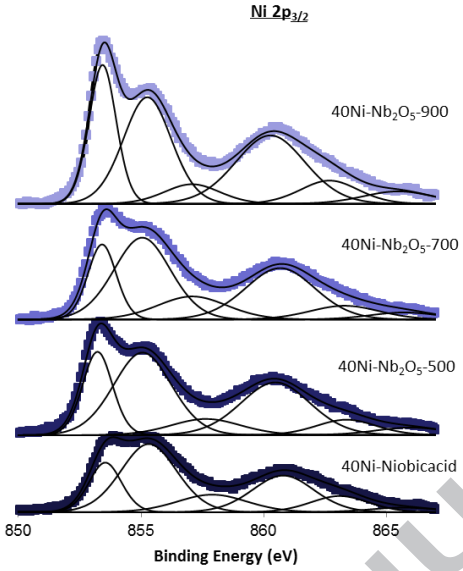

(b)

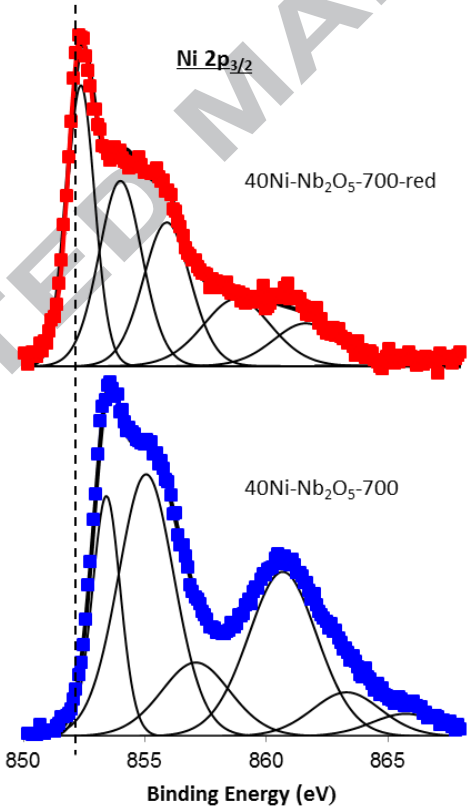

Figure 8

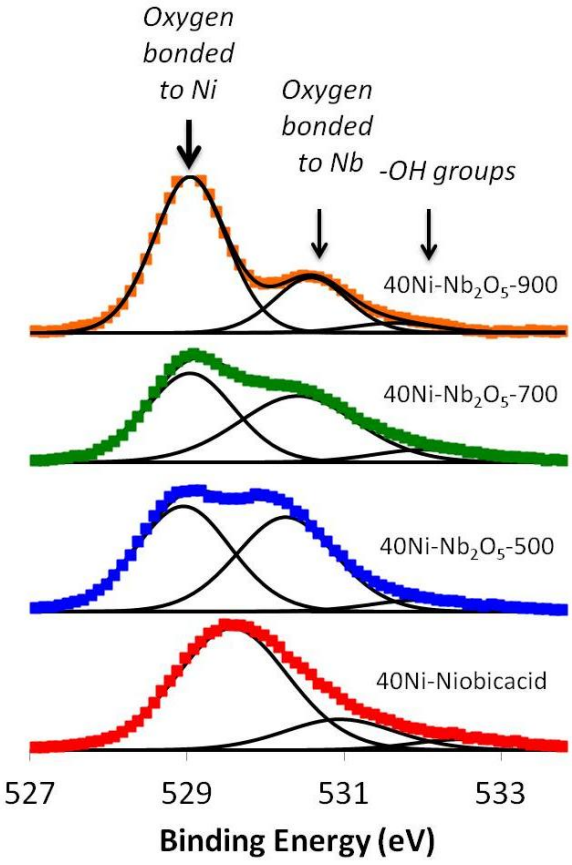

Figure 9

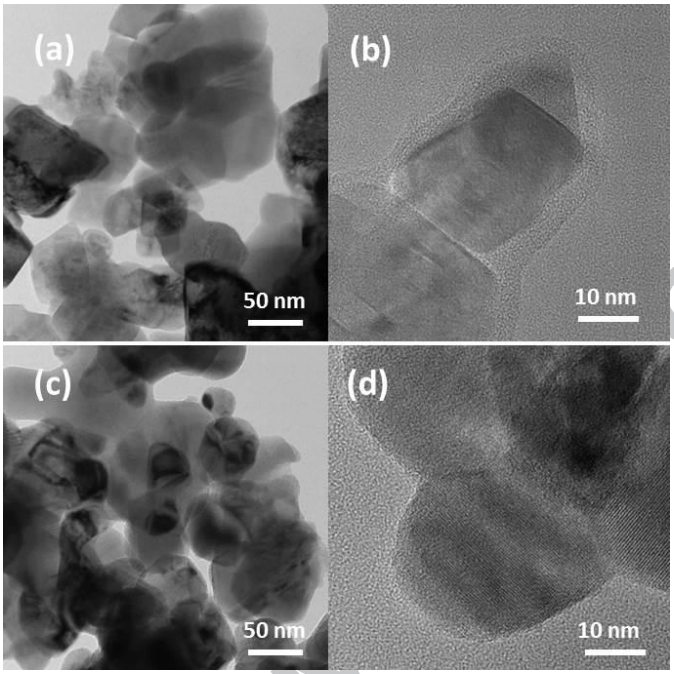

Figure 10

Graphical abstract

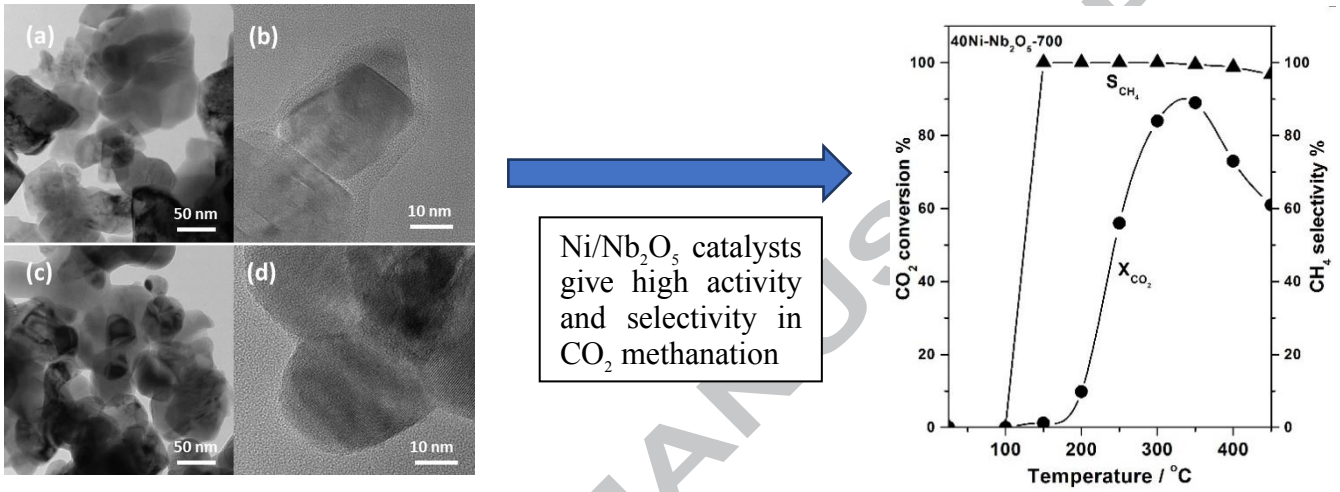

Graphical abstract

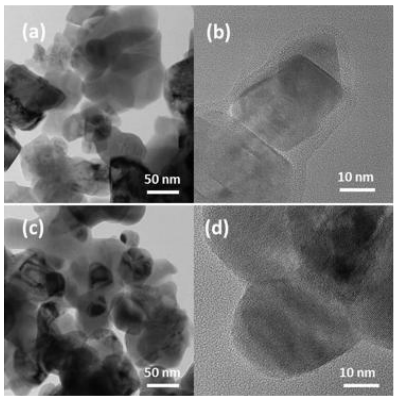

Ni–Nb_2O_5 catalysts give high activity and selectivity in CO_2 methanation

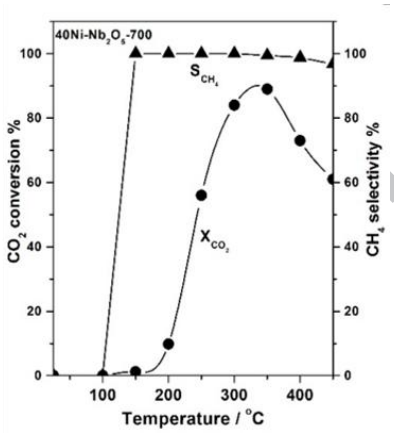

HIGHLIGHTS

- Heterogeneous catalysts based on nickel supported on niobia are synthesised.
- The catalysts are tested in CO_2 hydrogenation to methane in a packed bed reactor.
- The catalysts are active and highly selective in CO_2 methanation.
- A continuous test of 50 h confirmed the stability of the catalysts.
- The catalytic performance depends on the treatment temperature and niobia loading.